Global impact of ionospheric outflows on the dynamics of the magnetosphere and cross-polar cap potential

R. M. Winglee, D. Chua, M. Brittnacher, and G. K. Parks

Geophysics Program, University of Washington, Seattle, Washington, USA

Gang Lu

National Center for Atmospheric Research, Boulder, Colorado, USA

[1]   Statistical results for the ionospheric outflows indicate that the ionosphere is an important source of plasma to the magnetosphere. However, the exact consequences on the dynamics of the magnetosphere from this ionospheric outflow have yet to be determined. This issue is taken up in multifluid modeling of the 24−25 September 1998 magnetic cloud event for which strong heavy ionospheric outflows have been previously reported. It is demonstrated that one of the key influences of heavy ionospheric outflows is to lower the cross-polar cap potential due to the mass loading it produces on the magnetosphere; i.e., the heavy ions provide a major sink for momentum that is transferred from the solar wind to the magnetosphere. The derived values for the cross-polar cap potential are shown to converge to that attained by assimilated mapping of ionospheric electrodynamics (AMIE) as the O^+ concentration at the ionospheric boundary is increased to $\sim$50% of the H^+ concentration. The mass outflows produced in the model are comparable to the reported statistical values for the same level of Kp observed during the event. The position of the open-closed boundary is shown to be located progressively poleward with increasing O^+ concentration, and that the derived position at the higher O^+ concentrations best fits the Polar UVI images during the event. In addition, the model results shown that the heavy ionospheric ions provide a substantial sink for the energy input into the auroral oval as calculated by either UVI and AMIE. Thus ionospheric outflows are not just important in determining the source of the plasma in the magnetosphere, but have a clear role in controlling the global dynamics of the magnetosphere and the transport of solar wind energy and momentum through the magnetosphere.   *INDEX TERMS:* 2740 Magnetospheric Physics: Magnetospheric configuration and dynamics; 2736 Magnetospheric Physics: Magnetosphere/ionosphere interactions; 2753 Magnetospheric Physics: Numerical modeling; 2431 Ionosphere: Ionosphere/magnetosphere interactions (2736); *KEYWORDS:* ionospheric outflows, polar cap potential, simulations

1.   Introduction

[2]   The magnetosphere is supported by two sources of plasma with inherently different properties. One source is the solar wind, and the other is the ionosphere. The solar wind source is often identified by the presence of He^{++}, and *Lennartsson* [1987, 1992] has used the presence of these ions in ISEE 1 data to demonstrate that the plasma sheet always has a significant solar wind component. A possible manifestation of the entry of solar wind plasma into the magnetosphere is that the density of the plasma sheet appears to be well correlated with the solar wind density [*Terasawa et al.*, 1997; *Borovsky et al.*, 1997]. This correlation appears to be higher for northward interplanetary magnetic field (IMF) than for southward IMF.

[3]   However, the ionosphere is a significant source of plasma to the magnetosphere [*Johnson*, 1979]. Observations over nearly three decades by polar orbiting spacecraft indicate that the number fluxes are sufficient to support the observed densities in the tail current sheet [*Johnson*, 1979; *Chappell et al.*, 1987, 2000; *Yau and André*, 1997; *André and Yau*, 1997]. Further evidence for the strength of the ionospheric source comes from Geotail observations that show that O^+ can be present in the midtail lobe/mantle [*Mukai et al.*, 1994] and distant tail [*Hirahara et al.*, 1996; *Seki et al.*, 1996]. A statistical study by *Seki et al.* [1998] indicates that the lobe/mantle O^+ beams between 8 and 210 R_E have an average density during solar minimum of $\sim$1 $\times$ 10^{-3} cm^{-3}, which correspond to $\sim$1.2% of the proton component. At even this small concentration, O^+ is providing nearly 20% of the total mass density. During storms the oxygen concentration in the ring current can be comparable

to if not dominate that of H$^+$ [*Krimigis et al.*, 1985; *Hamilton et al.*, 1988; *Roeder et al.*, 1996].

[4] Given that there are significant components of both solar wind and ionospheric plasma in the magnetosphere, *Moore* [1991] and *Moore and Delcourt* [1995] have proposed that within the magnetosphere there is a boundary called the geopause, within which the dynamics is dominated by ionospheric plasma, and outside by plasma of solar wind origin. The geopause was envisaged to extend into at least the midtail region as suggested by single particle tracking [*Delcourt et al.*, 1989, 1993].

[5] Multifluid simulations by *Winglee* [1998a, 1998b, 2000] have been able to separate out the relative contributions of the ionospheric and solar wind plasmas as a function of the IMF. For northward IMF the simulations indicate that convection of field lines over the polar cap is relatively slow so that ionospheric outflows appear suppressed. In addition, solar wind plasma is able to enter through high-latitude reconnection and the subsequent convection of these mass-loaded field lines causes the solar wind plasma to be dispersed deep into the magnetosphere. As a result, the geopause for the northward IMF is relatively small.

[6] For southward IMF, reconnection tends to be restricted to the subsolar region, and while there is enhanced entry of solar wind plasma into the cusp, much of the solar wind plasma that is able to enter is convected into the deep tail, rather than into the near-Earth region. Simultaneously, the faster convection of the field lines over the polar cap and auroral regions causes stronger centrifugal acceleration of ionospheric plasma, thereby generating enhanced ionospheric outflows and causing the geopause to increase in size [*Cladis*, 1986; *Horwitz*, 1987; *Winglee*, 1998a, 1998b, 2000]. This change in the size of the geopause also appears to be consist with the statistical studies of *Terasawa et al.* [1997] and *Borovsky et al.* [1997] where the correlation of plasma sheet density with solar wind density is better for northward IMF than for southward IMF.

[7] In this paper we show that the outflow of heavy ionospheric ions can have a pivotal effect on the global dynamics of the magnetosphere. It is demonstrated that during disturbed times O$^+$ plays a crucial role in limiting the cross-polar cap potential and provides an essential energy sink for the power deposited into the ionosphere as seen by its auroral emissions. As a quantitative example, we model the magnetic cloud event of 24−25 September 1998 where the outflow of O$^+$ was observed to be sufficiently enhanced that it dominated the composition of the mantle [*Moore et al.*, 1999]. This event was accompanied by an increase in *Kp* from ∼3 to ∼7. In order to show the influence of the ionospheric outflows on the global dynamics, a series of simulations are presented. Each of the simulations is driven by the same solar wind conditions, but the ionospheric composition at the inner boundary is systematically varied and the corresponding global response is compared with estimates for the flux of the ion outflows, the cross-polar cap potential, size of the polar cap and auroral oval, and the total power into and out of the auroral zone.

[8] In the model without the presence of O$^+$ the cross-polar cap potential on average is a factor or 3 to 4 times higher than calculated from assimilated mapping of ionospheric electrodynamics (AMIE) [*Lu et al.*, 1996]. This discrepancy in the global model potential has been seen by

other MHD models where the plasma is treated as a single fluid [*Winglee et al.*, 1997; *Raeder et al.*, 1998; *Fedder et al.*, 1998]. In addition, the simulations with a tenuous ionosphere have an outflow rate substantially smaller than the statistical value determined by *Yau and André* [1997], and the power in the outflows is very much smaller than the power into the ionosphere as determined by the Ultraviolet Imager (UVI) on the Polar spacecraft and below the estimated Ohmic heating from AMIE. Hence there is a net imbalance in the mass and energy flow. With the inclusion of O$^+$ at relative concentrations comparable to the H$^+$ density, it is shown that the model number fluxes are comparable to the values given by the synthesis of various data sets by *Yau and André* [1997]. At the same time, the cross-polar cap potential as determined by the multifluid model is reduced to a value comparable to the AMIE result, and the discrepancy in between the power in and out of the ionosphere is diminished. The reduction in the cross-polar cap potential is also seen as a reduction in the polar cap area, and the size of the oval as determined by the model is comparable to that in the UVI images.

[9] These results all go to showing that the issue of the relative contributions of ionospheric and solar wind plasma is not just one of identifying sources. They have crucial influence on the structure of the magnetosphere and its dynamics, particularly during disturbed times.

2. Model Description

[10] The details for the numerical scheme and boundary conditions are given by *Winglee* [1998a, 1998b, 2000]. The equations are essentially the standard multifluid equations for a plasma with the ion and electron equations kept separate unlike MHD which combines the equations for a single-fluid description. The grid spacing increases from 0.4 R_E in the dayside and midtail regions, to ∼3 R_E in the distant tail at $x \sim -200$ R_E (GSM) and at the flanks at ±60 R_E. The solar wind boundary is at $x = 35$ R_E.

[11] The inner radius of the simulations is set to 2.4 R_E, which is typical of global simulation models. The dynamics of the outflow of ionospheric H$^+$ and O$^+$ ions is not only controlled by magnetospheric driving but also by the actual composition of the ionosphere that in turn is influenced by the Earth's gravity. In the actual ionosphere the low temperature (<1 eV) of the ionospheric ions is insufficient to allow them to overcome gravity and escape. Because the simulation boundary is limited to 2.4 R_E the actual gravitational force on oxygen would be negligible. Therefore, in order to model the gravitational confinement of low-energy heavy ions the simulations assume a heavy mass for the Earth so that the heavy ions in the simulations between the inner boundary and 1 R_E altitude experience essentially the same average gravitational force as an actual O$^+$ within 1 to 2 R_E. In other words, the gravity term $g = G M_E/R_E^2$ in the simulations is set at 30 m s^{-2} as opposed to its actual value of 10 m s^{-2}. This increase in the gravity enables the bulk of the O$^+$ ions near the inner boundary to be gravitationally bound and some additional acceleration, such as centrifugal acceleration, is required to drive heavy ion outflows into the magnetosphere. While the gravity term is 3 times higher everywhere, it had negligible effects on the dynamics of the magnetospheric flows since the corresponding force at high
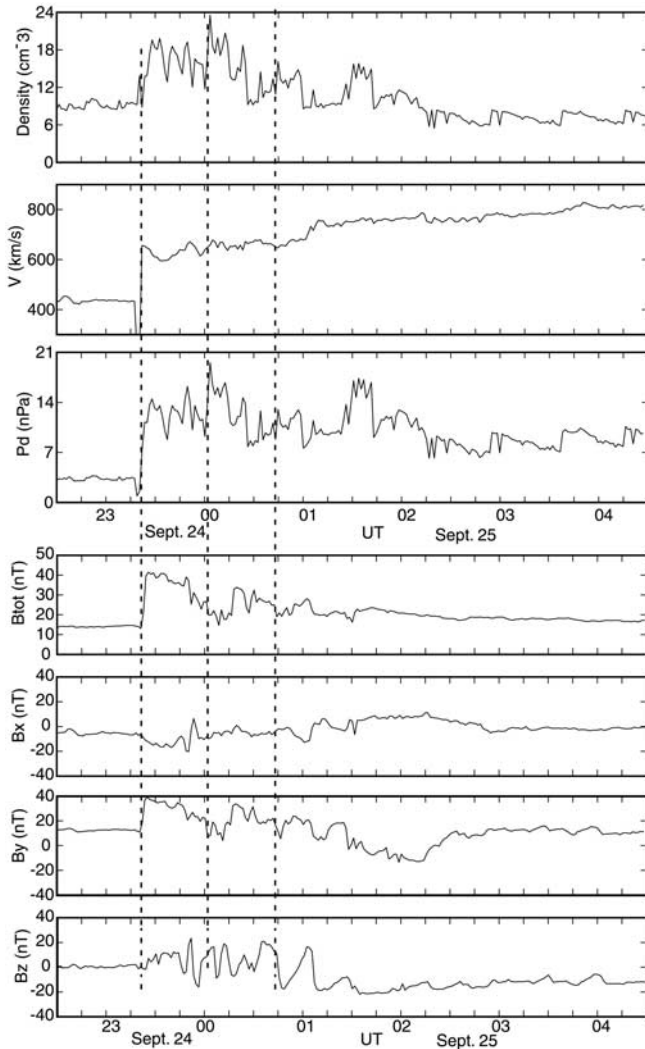
Figure 1. Solar wind conditions for the 25 September 1998 magnetic cloud event as observed by the Wind spacecraft which was 185 R_E upstream. The first dashed line indicates the arrival of the cloud, which is associated with a large increase in solar wind dynamic pressure during predominantly northward interplanetary magnetic field (IMF). The second dashed line indicates the starting of the period of sustained southward IMF.

altitudes (>5 R_E) is very much smaller than the $J \times B$ and grad P forces. Test runs with this value show that the outflow of oxygen is inhibited relative to the H$^+$ outflow when there is only weak forcing by the solar wind.

[12] In order to determine the effects of the ionospheric composition on the dynamics of the magnetosphere, each simulation is run with fixed ionospheric boundary conditions. The results from a series of such simulations are then compared to quantitatively determine the ensuing changes in the magnetospheric response. The nominal ionospheric H$^+$ density at the inner boundary is set at 400 cm^{-3} and as discussed in the next section leads to an outflow rate of the order of $\sim 0.5-2 \times 10^{26}$ ions s^{-1}, depending on solar wind conditions. This range is consistent with the range of H$^+$ fluxes reported by *Yau and André* [1997] at 0.5×10^{26} ions s^{-1} at $Kp = 3-0.9 \times 10^{26}$ ions s^{-1} at $Kp = 6$.

For comparison, a tenuous ionosphere is also considered with a density at the inner boundary of 100 cm^{-3}.

[13] O$^+$ densities at the inner boundary used in the following simulations range from 5 to 100% of the H$^+$ density. These boundary conditions produce O$^+$ outflows of the order of $0.2-7 \times 10^{26}$ ions s^{-1}. This outflow range spans the range of 0.6×10^{26} ions s^{-1} at $Kp = 3-2 \times 10^{26}$ ions s^{-1} at $Kp = 6$ estimated by *Yau and André* [1997].

[14] The pressure along each flux tube is initialized as a constant value (set by mapping the simulation grid point along the dipole field line to the equator and giving all points along the field line the value prescribed to the equator). The equatorial bulk temperature is set to ~ 60 eV and in the polar cap it is less that 0.3 eV. The low temperature over the polar cap ensures that much of the ionospheric O$^+$ is gravitationally bound, while the higher temperature at the equator incorporates the fact that on closed field lines, hotter plasma can be trapped and lead to a higher overall equatorial temperature. The assumed value gives approximately the same total plasma pressure for the region when both the plasmaspheric and ring current contributions are included.

[15] Figure 1 shows the solar wind conditions for the event as observed by the Wind spacecraft, which was ~ 185 R_E upstream. These solar wind conditions are used to drive the simulations. Prior to the arrival of the magnetic cloud, the solar wind conditions are close to the nominal with a density of $7-8$ cm^{-3} and a speed of 430 km s^{-1}. The Kp at this time is ~ 3. With the arrival of the shock at Wind at ~ 2325 UT the density jumps by a factor of 2, and the speed increases to $600-650$ km s^{-1}, producing an increase of nearly a factor of 4 in the solar wind dynamic pressure. At 600 km s^{-1} the propagation time to Earth is ~ 33 min. As the event proceeds, the wind speed gradually increases to ~ 800 km s^{-1} and the corresponding propagation time is reduced to 25 min.

[16] The IMF for this period is shown in the lower part of Figure 1. Prior to the arrival of the magnetic cloud, the IMF is dominated by a strong (10 nT) duskward field. With the arrival of the magnetic cloud, IMF B_y remains the dominant component with its magnitude increasing by nearly a factor of 3. Between 0045 and 0110 UT, there is a transition to a strongly southward (< -15 nT) IMF. It is demonstrated in the following that the ionospheric response to the arrival of the pressure pulse and the subsequent 1 hour of activity is different from that driven by the sustained southward IMF, with the ionospheric ions possibly playing the greatest role in the later period [*Moore et al.*, 1999]. The magnetic cloud causes the Kp to increase to 7.

3. Size of Ionospheric Outflows

[17] In order to determine the flow of ions out of the magnetosphere as a function of both the ionospheric boundary conditions and the forcing from the solar wind, we integrate the flux crossing a surface set at 6 R_E. The height of 6 R_E is chosen to ensure that this calculated outflow is likely to move out into the plasma sheet and deep tail and avoids possible confusion of just motion of the ionospheric ions as opposed to actual outflow.

[18] The calculated outflows for the nominal and tenuous ionospheres are shown in Figure 2. It is seen that the
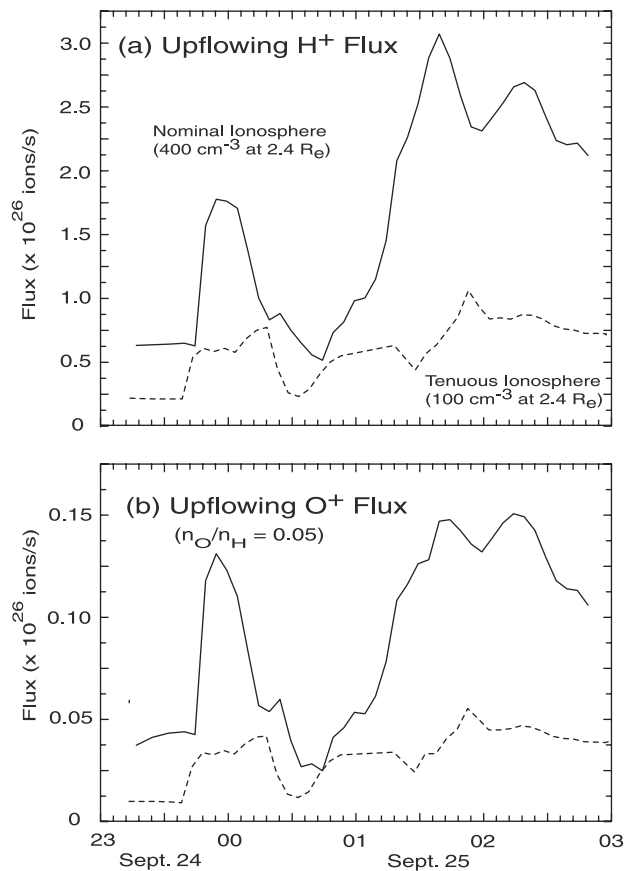
Figure 2. The ion outflow flux for the tenuous (H$^+$ density of 100 cm^{-3} at the inner boundary) and nominal (400 cm^{-3}) model ionospheres. Both have an O$^+$ relative density at the inner boundary of 5%. The total number flux for the tenuous ionosphere is much smaller than the values given by *Yau and André* [1997]. The nominal ionosphere also under predicts the value of the O$^+$ flux.

outflows for the tenuous ionosphere model (dashed lines) produces approximately H$^+$ outflows of ~0.2−1 × 10^{26} ions s^{-1}, which is comparable to the value give by *Yau and André* [1997] for the *Kp* levels for the event. However, the corresponding oxygen outflow (Figure 2b) at only 0.02−0.05 × 10^{26} ions s^{-1} is substantially smaller than the *Yau and André* [1997] results. The nominal ionospheric model (solid line) gives rise to stronger outflows in both H$^+$ and O$^+$ that are approximately proportional to the increase in density at the inner boundary. With this increase the total ion outflow in terms of ions s^{-1} is comparable to *Yau and André* [1997], but the mass flux in terms of kg s^{-1} is too small, i.e. there is too much H$^+$ and too little O$^+$.

[19] The macroscopic effect as calculated from the modeling from having too little ionospheric mass outflow can be seen by comparing the calculated cross-polar cap potential for the event with that derived from AMIE. The data inputs to AMIE for this particular event were obtained from 6 SuperDARN HF radars, 4 DMSP and 3 NOAA satellites, and 131 ground magnetometers distributed worldwide. The results in Figure 3 show that the tenuous ionosphere leads to a cross-polar cap potential, which is typically a factor of 2 larger than the AMIE results. The nominal ionosphere with

its higher ionospheric outflow produces a reduction in the cross-polar cap potential so it is only ~1.5 times the AMIE value. In other words, increases in the ionospheric outflow can reduce the cross-polar cap potential, but without significant O$^+$ outflow the calculated value is still higher than that inferred from AMIE.

[20] This reduction in the cross-polar cap potential can be understood as follows. The magnetosphere has an approximately fixed cross section exposed to the solar wind, so that there is a fixed amount of momentum coupled to the magnetosphere. As more mass is added to the magnetosphere through ionospheric outflows, the fixed amount of momentum means that the plasma on average convects slower in the magnetosphere. Since the convection speed of the plasma sets the convective electric field, which in turn sets the bulk of the cross-polar cap potential, the latter is seen to decline as larger ionospheric outflows occur. Thus ionospheric outflows have the macroscopic effect of limiting the maximum value of the cross-polar cap potential that a magnetosphere can attain.
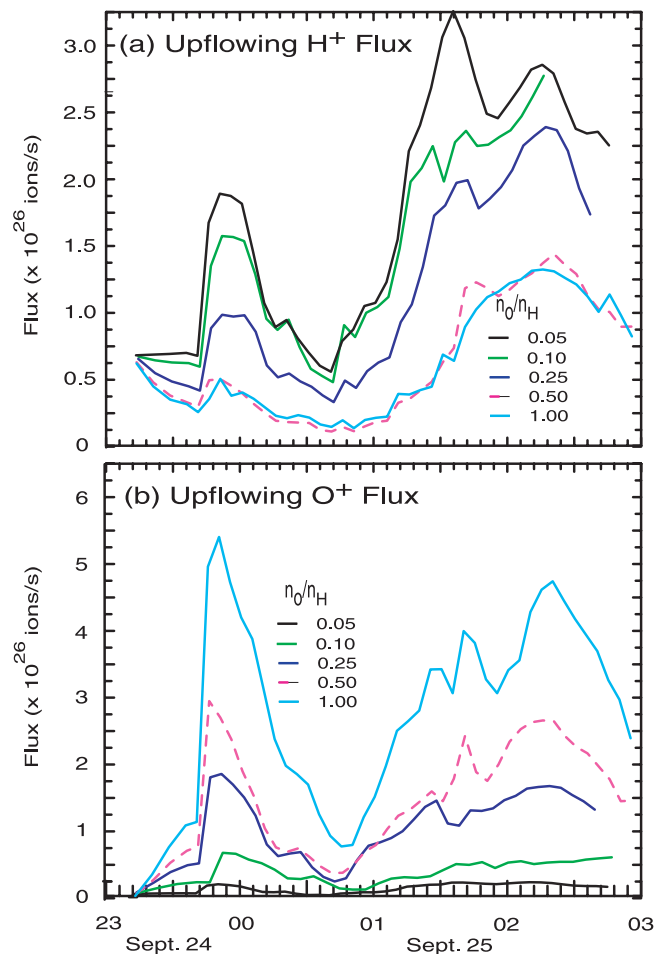

Figure 3. Changes in the outflow rates for varying O$^+$ ionospheric concentrations. As the O$^+$ concentration increases, the H$^+$ outflow decreases to its thermal limit. At about the 50% ionospheric concentration the calculated fluxes for both the H$^+$ and O$^+$ ions are comparable to the statistical results of *Yau and André* [1997] for the *Kp* values seen during event.
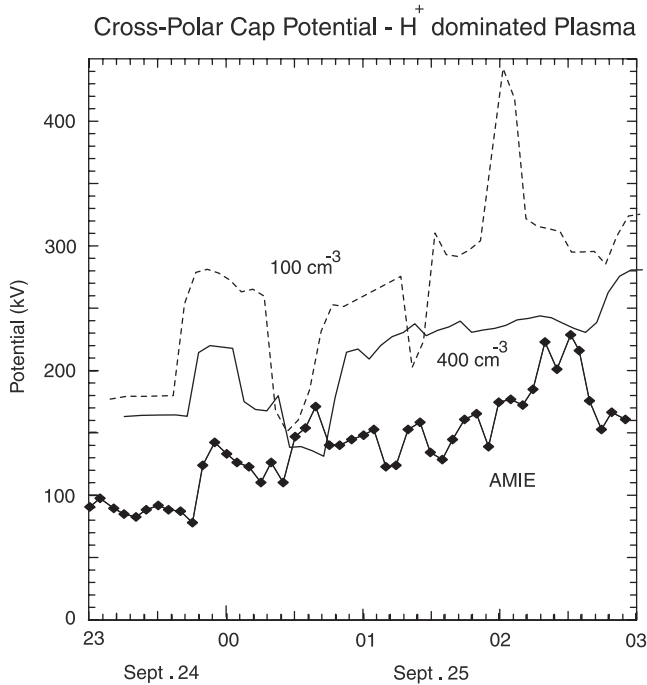
Figure 4. Comparison of the evolution of the cross-polar cap potential for tenuous and nominal ionosphere with that given by assimilated mapping of ionospheric electrodynamics (AMIE). With increased ionospheric outflow facilitated by the higher ionospheric density, the model potential is seen to decrease but is still significantly higher than the AMIE values.

[21] There is also feedback between the ionospheric outflows due to the changes in the cross-polar cap potential. This is partially seen in Figure 2 where the time histories for the outflows from the tenuous and nominal ionospheres do not reach their maximum and minimum values simultaneously. For example, for the arrival of the pressure pulse associated with the leading edge of the magnetic cloud ($\sim$0000 UT), the ionospheric outflow peaks earlier and has a slower decay time for the nominal ionosphere than for the tenuous ionosphere. For the period of sustained southward IMF it is difficult to correlate features between the different time profiles. In Figure 3 the feedback produces lags in the appearance on minima and maxima in the potential.

[22] The feedback between the ionospheric outflow and cross-polar cap potential becomes more evident as the relative concentration of O^+ is increased. To illustrate this effect, we performed a series of simulations where the H^+ density of the nominal ionosphere is held fixed and the O^+ is increased from 5 to 100% of the H^+ density at the inner boundary of the simulation. Since this O^+ is set as an inner boundary conditions and is not actually loaded into the magnetosphere, its presence in the magnetosphere can only be produced by outflows from the inner boundary. The corresponding time histories for the outflows for five different relative concentrations are shown in Figure 4.

[23] As the O^+ density is increased at the inner boundary, it is seen that O^+ outflow increases from $\sim 0.3 - 3 \times 10^{26}$ ions s^{-1}. These levels are comparable to the values given by *Yau and André* [1997]. Note that the assumption that the

density of O^+ needs to be approximately equal to the H^+ density is consistent with the observations of *Moore et al.* [1999], which show that the outflows for the event where indeed dominated by heavy ionospheric ions.

[24] The other important feature that can be seen in Figure 4 is that as the O^+ at the inner boundary is increased, the magnitude of the outflow of H^+ decreases despite the fact that the H^+ boundary conditions are held fixed. Note that there is a lower limit to the reduction with the two curves for H^+ outflows at $n_O/n_H = 0.5$ and 1.0 being approximately the same. At this level the range in the H^+ flux of $0.3 - 1.0 \times 10^{26}$ ions s^{-1} is comparable to that *Yau and André* [1997].

[25] The magnitudes of the ionospheric outflows are set by two factors in the model. The first is the thermal outflow (essentially the polar wind limit) that is determined by the density at the inner boundary, the temperature of the plasma there, and gravity. These flows are subject to centrifugal acceleration, which is the dominant component in the model, and this secondary acceleration leads to higher fluxes at higher altitudes. Centrifugal acceleration in turn is related to the cross-polar cap potential and is therefore highest with low ionospheric mass loading, i.e., when the O^+ relative concentration is low. As the O^+ concentration increases, the O^+ outflow rate correspondingly increases, but as it does so it decreases the cross-polar cap potential and for both the H^+ and O^+ ions the amount of centrifugal acceleration decreases. As a consequence, the O^+ flux at the higher concentrations does not increases as fast as the forcing at the inner boundary and the H^+ flux reaches a
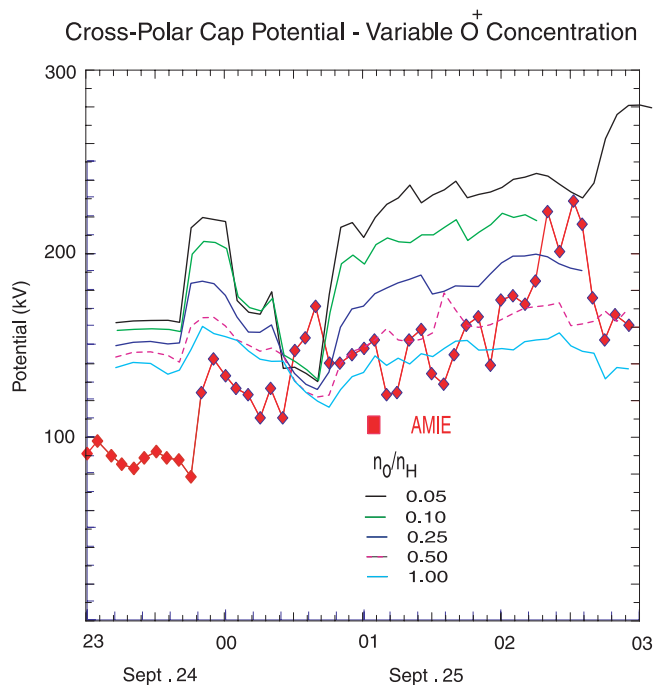

Figure 5. As in Figure 4, but for the nominal ionosphere with different relative concentrations of O^+. The model values converge onto the AMIE result as the relative density increases to $\sim$50%. The discrepancy at early times is due to insufficient time for the assumed O^+ to fully propagate out into the magnetosphere.
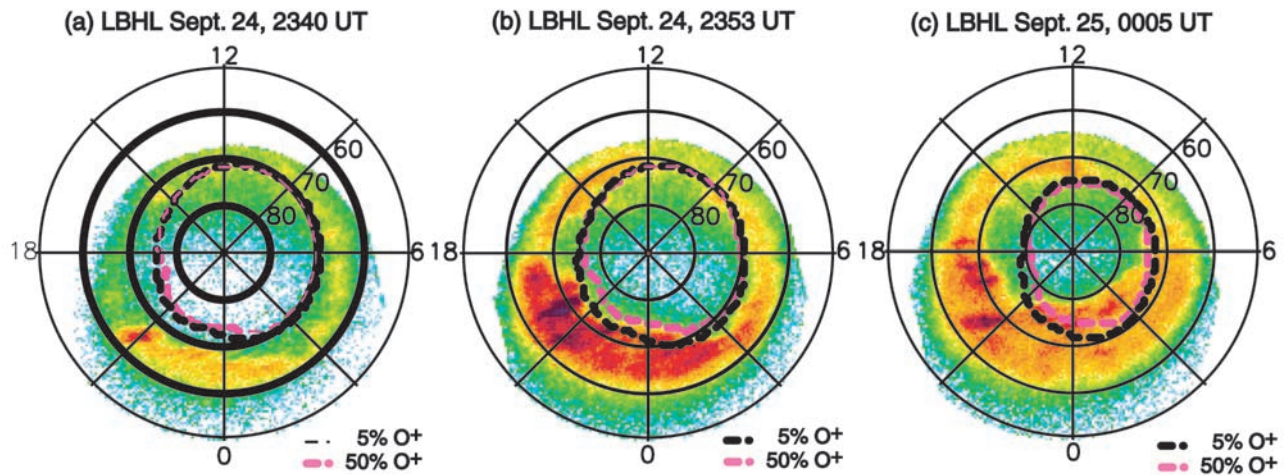
Figure 6. The aurora response produced by the arrival of the magnetic cloud as seen by Polar UVI. Superposed on the UVI images are the model open/closed boundaries for the nominal ionosphere with 5 and 50% O^+ concentration at the inner boundary. The self-limiting of the cross-polar cap potential by enhanced O^+ ionospheric concentrations is seen as the open/closed boundary moving in to higher latitudes (more closed) for the higher O^+ concentration.

minimum level that corresponds to their thermal outflow limit.

[26] The reduction of the cross-polar cap potential as a function of O^+ concentration is shown in Figure 5. As already noted, the presence of low O^+ densities at the inner boundary leads to limited mass outflows but at elevated speeds, and as a result the calculated cross-polar cap potential is ~50% above the level estimated by AMIE. At the higher concentrations the model potentials decrease and approach an average value comparable to that of AMIE. The main difference is at early times when the model indicates higher potentials. This discrepancy is due to the fact that the ionospheric outflows have had insufficient time in the simulations to fully permeate through the entire magnetosphere to produce any significant mass loading. As a result, the low level of mass loading leads to higher magnetospheric flow velocities and higher cross-polar cap potentials in the model at early times.

4. Auroral Oval Characteristics

[27] The above results indicate that the presence of strong O^+ outflows can limit both the H^+ outflows seen at high altitudes and the cross-polar cap potential. These outflows also have macroscopic effects on the dynamics of the auroral oval. One such property is the position of the open/closed boundary as illustrated in Figure 6. Data from UVI are plotted at three different times corresponding to just prior to the arrival of the cloud, the time of peak activity associated with the initial pressure pulse and the subsequent expansion of the auroral oval. Superimposed on these UVI images are the positions of the open/closed boundary as determined from the modeling for the nominal ionosphere with a relative oxygen concentration of 5% (black dashed curve) and 50% (dashed gray curve).

[28] It is seen that the effect of high O^+ concentrations in the ionosphere is to move the open/closed boundary poleward, particularly in the midnight sector. The shift is smallest at $1°-2°$ when the activity is relatively weak and the boundary for the lower concentration is probably the best fit with the UVI images. With increased activity the open/closed boundary for the higher O^+ concentration moves more poleward by $3°-4°$ and more closely tracks the UVI images (Figure 6b), but even at 50% concentration does not move far enough poleward to fully account for the small polar cap area that is associated with the recovery phase (Figure 6c).

[29] While the open/closed boundary gives some indication of the reconfiguration of the magnetosphere during these periods of auroral activity, it does not provide any information on the thickness of the auroral oval and the corresponding changes in the magnetosphere. In order to investigate the possibility of any such links we mapped several global quantities back into the auroral region to determine which tail features gave the best correlation with the UVI data. The quantities considered include the field-aligned currents, the energy influx from solar wind particles, the number and energy flux of the ionospheric outflows, and finally the energy distribution of the ionospheric ions in the magnetosphere. Only the latter parameter had an ionospheric mapping bore any resemblance to the UVI images.

[30] As an example, Figure 7 shows six UVI images starting just prior to the arrival of the cloud and extending 2 hours later when the IMF was predominantly southward. Superposed on these images are contour maps of the maximum temperature of the ionospheric ions mapped along the field lines. The ionospheric plasma instead of the solar wind component is used because it has the higher temperature inside the magnetosphere and avoids confusion from heated plasma within the magnetosheath. Since the UVI colors represent fixed intensities, the contours of the temperature profiles are also held fixed. The highest temperatures are correlated with the tail, and prior to the arrival of the cloud, they are limited to a restricted range of MLT (from ~2100 to 0300 MLT) and MLAT ($60°-70°$), similar to the UVI observations. The main difference with the UVI
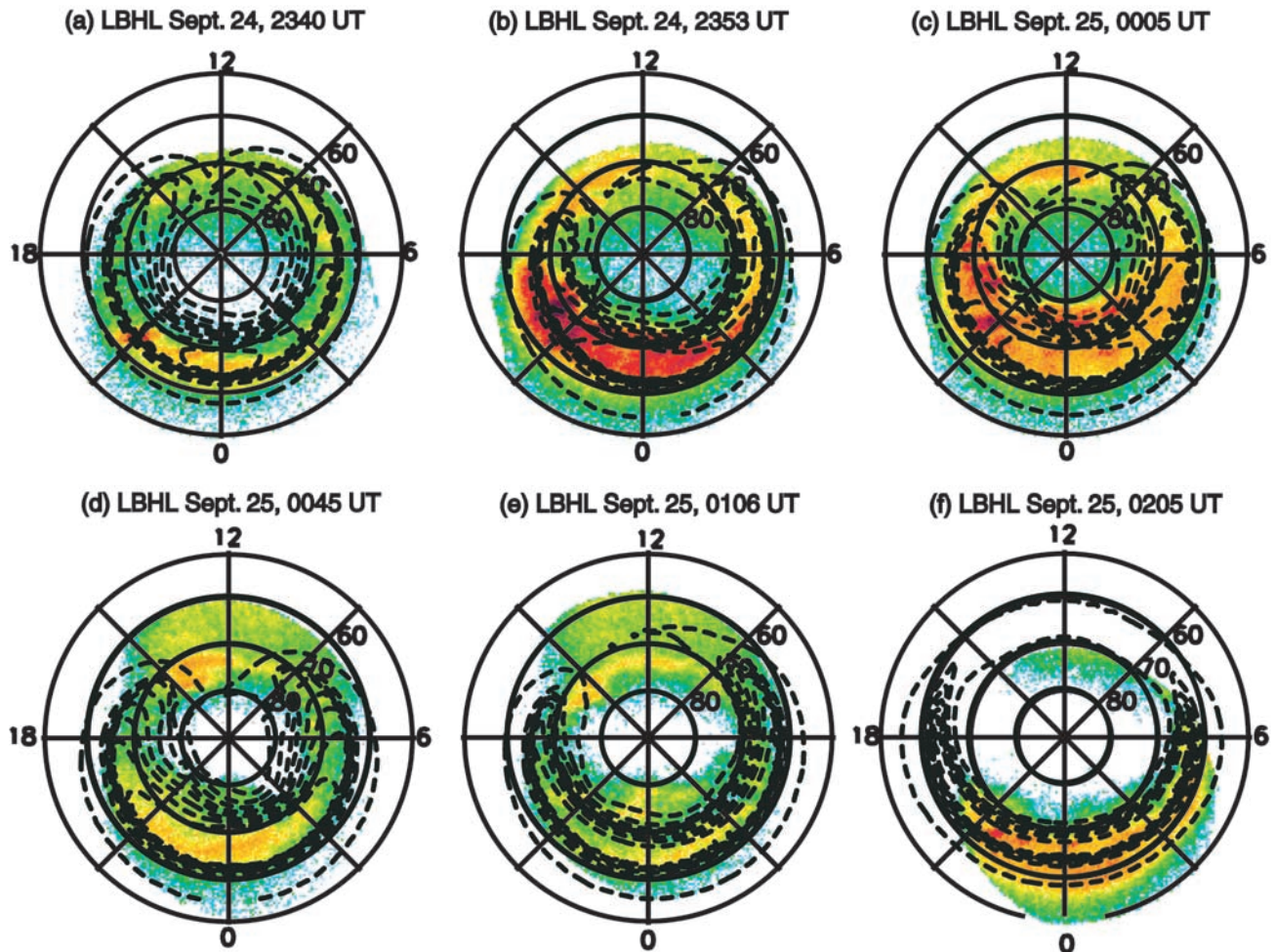
Figure 7. Polar UVI images covering the initial arrival of the cloud and the extended period of southward IMF. Superimposed are contours of the model maximum temperature (essentially equatorial temperature) of the ionospheric ions along the field lines. It is seen that these contours provide a good proxy for the enhancements in the UVI emissions.

observations is that there is a localized bright spot in the UVI observations around 2100 MLT that is not seen in the simulations.

[31] With the arrival of the cloud, not only does the auroral oval appear brighter but it is broader in both MLT and MLAT. This broadening of the region is also seen in the temperature contours over essentially the same regions (Figures 7b and 7c), including the expansion of the auroral into the polar cap. The presence of a small polar cap and high tail temperatures is sustained for nearly 45 min after the arrival of the cloud. With the turning of the IMF to predominantly southward the polar cap as seen in the UVI data is seen to again expand (Figures 7e and 7f) beyond its initial size observed prior to the arrival of the cloud. This same expansion over essentially the same MLT and MLAT occurs in the temperature contours derived from the model.

5. Magnetospheric Distribution of Plasma

[32] The relative concentration of O^+ in the magnetosphere that develops from the ionospheric outflows is illustrated in Figure 8 for the case of 50% concentration

(the distributions for the other assumed ionospheric concentrations are similar scale according to the assumed concentration at the inner boundary). As noted earlier, even though we assume a high O^+ concentration at the inner boundary just prior to the arrival of the cloud, it does not have time to convect throughout much of the magnetosphere. As a result, the O^+ concentration is below the 1% level except in the near-Earth region. The pressure pulse (Figure 8a) causes a compressional wave that leads to high concentrations in the near Earth midnight sector. With the sustained southward IMF, convection of the dayside O^+ ions leads to lobe concentrations into the deep tail of a few percent concentration. This level is consistent with the typical values of O^+ seen in the distant tail [*Hirahara et al.*, 1996; *Seki et al.*, 1996]. As noted in the introduction, at even a few percent concentration, the O^+ ions are providing several tens of percent of mass and therefore are significant to the overall transfer of momentum from the solar wind to the magnetosphere. Figure 8 also shows that the nightside O^+ outflows provides a distinct plume that feeds the inner current sheet with concentrations varying from 15 to 50% in the near-Earth region. As such, this mass loading will play
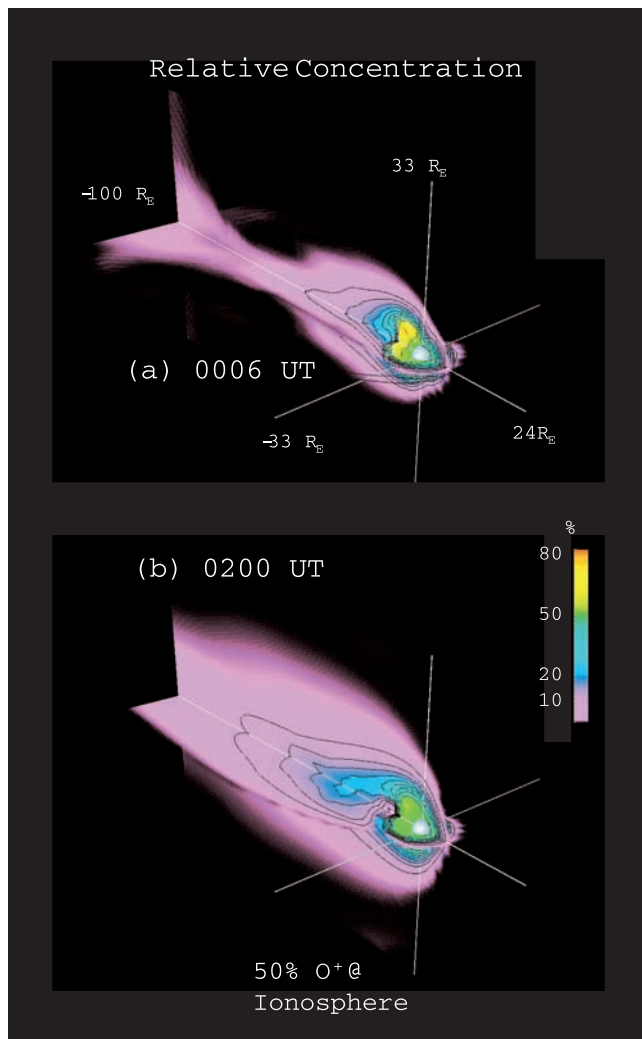
Figure 8. Relative concentration of O^+ in the magnetosphere for the event as determined by the model at (a) 0006 UT shortly after the arrival of the pressure pulse and (b) at 0200 UT during the period of sustained southward IMF. The ionosphere is assumed to have a 50% O^+ concentration at the inner boundary.

an important role in the tail energetics, particularly since some of this O^+ is flowing directly into the reconnection region.

[33] Figure 9 shows the extent in the magnetosphere of the hot plasma regions identified in the auroral maps in Figure 7. The magenta regions indicate regions either where the temperature is below 1 eV or where the density is below 0.01 cm^{-3}. Prior to the arrival of the cloud, the hottest region is associated with ionospheric plasma that flows out of the midnight sector and is adiabatic heated as it is convected into the near-Earth plasma sheet. Some of this heated plasma is convected down the tail with little change in MLT. The other component of this heated plasma is convected around the flanks toward the terminator. As it approaches the LLBL, this component is also convected down the tail. Because of the different convection paths of this hot plasma, there is an actual temperature minimum region in the midtail region on either side of local midnight.

[34] The arrival of the magnetic cloud produces adiabatic heating of the near-Earth region, producing the broader hot region in the tail as well as its extension into the dayside (Figure 9b). The temperature minimum is again present but appears shifted by several R_E in y due to the broadening of the hot component near midnight. As the cloud front moves down the tail (Figure 9c) the dayside component cools while there is continued heating of the tail near local midnight. This hot component is seen to extend beyond the 100 R_E shown in Figure 9. About 40 min after the arrival of the cloud (Figure 9d) the deep-tail energetic component is lost from the system, but there is still a hot component in the near-Earth region that is larger in the near-midnight region than seen in the precloud magnetosphere. In addition, the flank component is more strongly depleted of hot ionospheric plasma.

[35] The temperature profile attained in the magnetosphere is influenced by the outflow of heavy ionospheric ions as illustrated in Figure 10. The left-hand side shows the H^+ and O^+ ion temperatures for 5% oxygen at 15 min after the arrival of the cloud, while the right-hand side shows the profiles at the same time but for 50% concentration at the ionospheric boundary. It is seen that for the H^+ ions the maximum ion temperature for the two different cases are approximately the same. The main difference is that distribution of hot plasma across the tail is reduced by ~20% in width for the higher oxygen concentration.

[36] The most prominent difference in the temperature profile for the O^+ ions is that with increased O^+ concentration at the inner boundary the cusp/cleft source there is greater penetration at higher latitudes. This greater penetration leads to O^+ being the dominant source of hot plasma in the mantle. This result is consistent with the in situ observations of *Moore et al.* [1999].
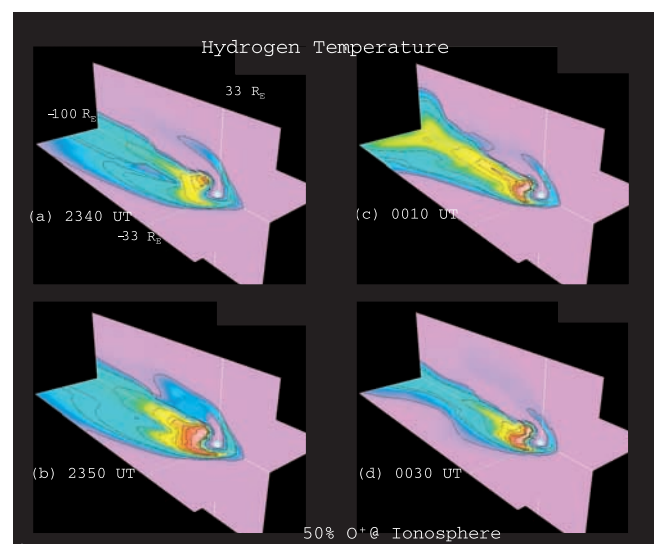

Figure 9. Equatorial and noon-midnight meridian cuts of the ionospheric H^+ temperature corresponding to the mapping of Figure 7. The pressure pulse produces adiabatic heating of the plasma sheet that moves down the tail. However, the middistant tail cools relatively fast, leaving the inner magnetosphere strongly heated after the passage of the pressure pulse.
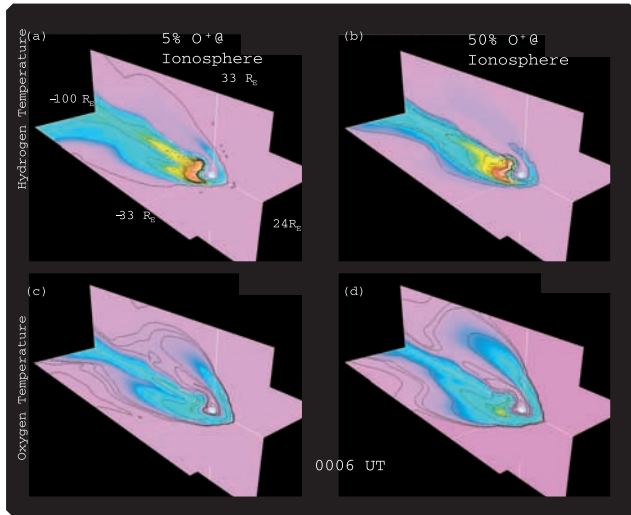
Figure 10. Changes in the (top) H$^+$ and (bottom) O$^+$ temperature profiles for the nominal ionosphere with O$^+$ at the inner boundary equal to (left) 5% and (right) 50%. The region of hot magnetospheric H$^+$ decreases with increasing O$^+$ ionospheric concentrations, while the region of hot magnetospheric O$^+$ increases both at high and low latitudes.

[37] For the plasma sheet, there are two effects seen arising from the increased O$^+$ concentration in the iono- sphere. First, there is an increase in the temperature of O$^+$ ions in the midnight sector. Second, there is a substantial increase in the width in which hot O$^+$ ions are seen across the tail. These variations in the spatial distributions are a direct consequence of the changes the O$^+$ ions produce in the cross-polar cap potential. The potential is large enough to cause efficient centrifugal acceleration of plasma out of the ionosphere, and the associated convection allows the outflows to experience additional heating and acceleration in the near-Earth current sheet. It is interesting to note that if the O$^+$ outflows did not reduce the cross-polar cap potential (from the 200+ to ~120 kV), much of the O$^+$ be rapidly transported into the deep tail before it experiences secondly current sheet acceleration. It is the feedback between the outflows and the cross-polar cap potential that enables O$^+$ to be the dominant source of hot plasma in the mantle and in the near-Earth current sheet.

6. Energy Deposition

[38] Another independent method to test for the signifi- cance of heavy ionospheric outflows is to perform an energy balance between the energy input into the ionosphere and the energy output carried by the ionospheric outflows. While the energy input and output may differ over limited timescales, a sustained imbalance would mean that there would be strong heating of the ionosphere but such heating would inevitably produce enhanced outflow of ionospheric plasma and thereby eliminate the imbalance. There are two methods to determine experimentally the power input into the ionosphere. One method is to use the UVI data emis- sions to calculate the power in the precipitating electrons generating the observed UV emissions. Estimates from this method are only available during the period when UVI is able to see the entire auroral oval. For the present event the UVI energy deposition estimates are from ~2320 to 0120 UT. The other method is to use the AMIE potentials and currents to calculated the total Ohmic heating [*Lu et al.*, 1996]. The later estimates have the advantage that they are available through the entire period of interest.

[39] The power inferred from AMIE and UVI is shown in Figure 11. The overall time profiles from the two methods agree fairly well except that AMIE shows an increase in the Ohmic heating around 0030 UT that has no counterpart in the UVI data. In addition, the Ohmic-heating rate is about twice that of the UVI electron precipitation energy. This difference is consistent with that already noted by *Lu et al.* [1996] and is due to the fact that the UVI data only provide information on the electrons of sufficient energy to produce the UVI emissions and neglects the low-energy component of the electrons that support the currents and drive the Ohmic heating in the ionosphere.

[40] Irrespective of the method of the calculation, the arrival of the cloud leads to the deposition of an additional 300–500 GW into the ionosphere. There is then an expo- nential-like decay in this additional energy deposition with an e-folding period of ~20 min. During the period of sustained southward IMF (starting at ~0130 UT) the energy deposition in the ionosphere increases to a peak of ~1000 GW.

[41] In order to measure the power output in the model ionospheric outflows, we integrated the particle energy fluxes at the 6 R_E boundary used to calculated number flux.
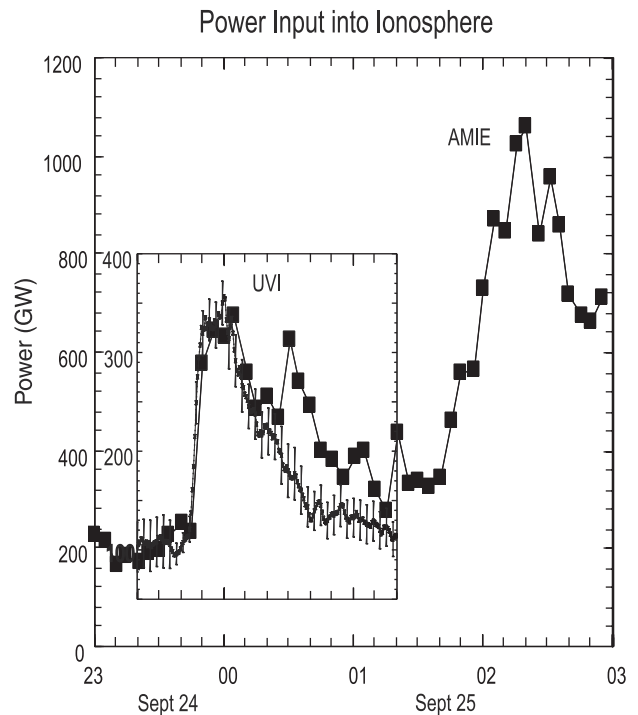

Figure 11. The energy deposition as determined by Polar UVI from precipitating electrons and from AMIE associated with Joule heating. The shapes of the curves are very similar, but there is approximately a factor of 2 in the total power due to differences actual quantity being calculated.
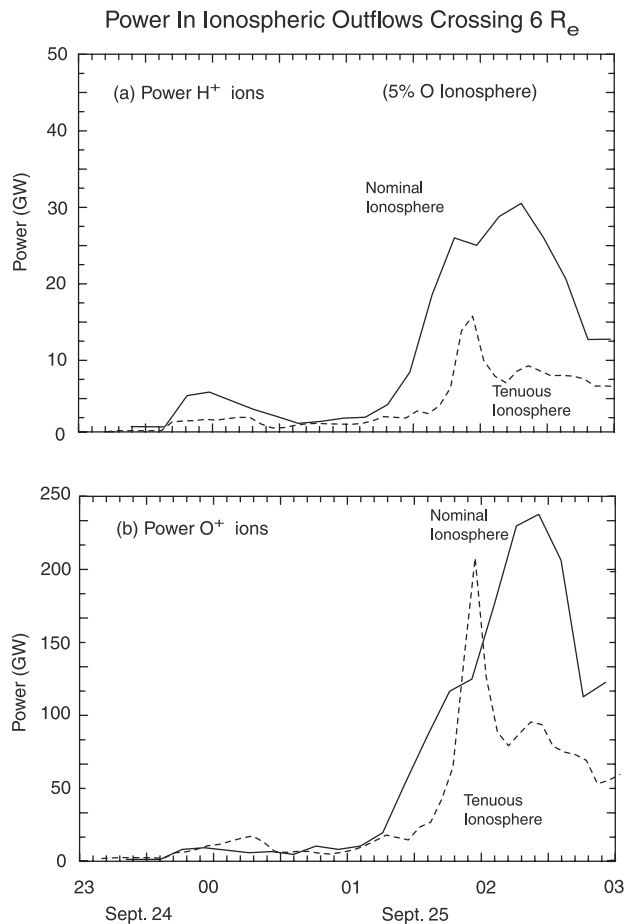
Power In Ionospheric Outflows Crossing 6 R$_e$

Figure 12. Power in the ionospheric outflows crossing 6 R_E for the tenuous and nominal ionospheric models. Even though in both cases O$^+$ is only a minor species at 5% at the ionosphere boundary, it is a significant energy sink. Without its presence, there is too little power in the H$^+$ outflows to account for the powers calculated from UVI and AMIE.

As noted in section 3, this height allows us to calculate fluxes most likely to reach the plasma sheet and deep tail, while avoiding possible confusion from inner boundary conditions changes. Because of the extended height at which the flux is calculated, there should be time delays between the UVI/AMIE power input and the model power output calculated at 6 R_E. In addition, the model power output is expected to be lower that the UVI/AMIE results since not all the power from the latter methods is expected to reach 6 R_E. Therefore, to provide an addition test for the modeling, we investigate whether there are significant (< 10%) and extended discrepancies (>60 min) relative to UVI/AMIE for the different assumed ionospheric boundary conditions. Large discrepancies would be suggestive of insufficient ionospheric outflow.

[42] Figure 12 shows the model power output from the ionospheric outflows for the tenuous and nominal ionospheres. It is seen that the power in the H$^+$ ions while having a similar shape as the UVI/AMIE curves in Figure 11, has a magnitude of only ~1% of the UVI value and ~0.5% of the AMIE result. Thus there is a gross imbalance between the

input and output energies for an ionosphere with only H$^+$ is present.

[43] Figure 12 (bottom) shows the power in the O$^+$ ions for the tenuous and nominal ionospheres, both of which have a 5% O$^+$ concentration. The O$^+$ power has two local maximum like the H$^+$ ions but the strength of the second peak is relatively much stronger. During the period of the initial arrival of the cloud the O$^+$ ions carry nearly twice the energy of the H$^+$ ions even though they are 5% of the number density. They are able to do so because the ions are approximately covelocity, which means that with their higher mass they are able to carry a significant fraction of the power. They are actually able to carry even more energy that the H$^+$ ions because convection of heavy ions from the dayside into the nightside leads to local enhancements in the O$^+$ ions in the midnight sector where most of the energization of ionospheric plasma is occurring. Nevertheless, while the O$^+$ ions are the main energy sink, during the initial pressure pulse the ionosphere does not have sufficient time to react and there remains a substantial power imbalance.

[44] However, during the extended period of southward IMF the ionospheric outflow is able to catch up with the energy input into the ionosphere, and for the nominal ionosphere, there is a sustained outflow of ~250 GW in O$^+$ and ~30 GW in H$^+$. The tenuous ionosphere is unable to keep up and only manages a sustained output of ~100 GW in O$^+$ and 7.5 GW in H$^+$.

[45] The effect on the power outflow as the ionospheric O$^+$ concentration is increased is shown in Figure 13. It is
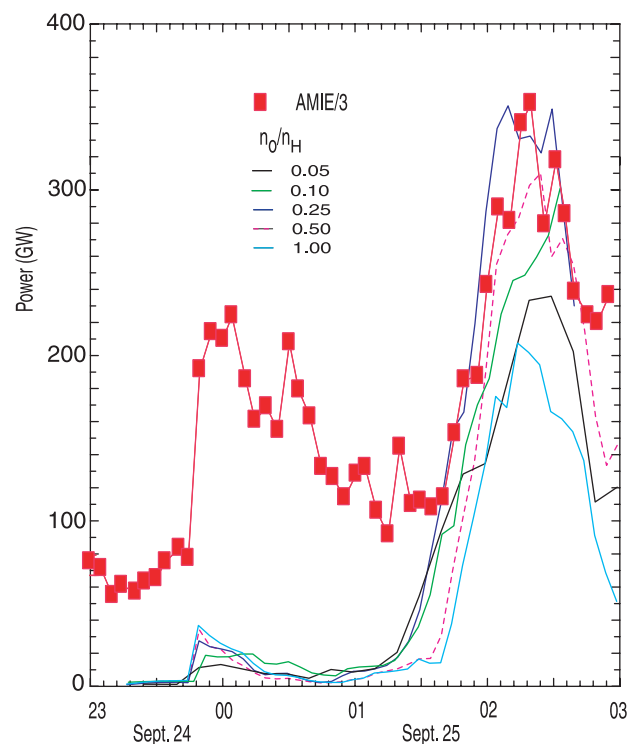

Figure 13. Total power out in the ionospheric outflows as a function of ionospheric O$^+$ concentration. Because the O$^+$ ions modify the cross-polar cap potential, the power reaches a maximum of ~1/3 the AMIE value at concentrations of between 25 and 50%.

seen that while the O^+ concentration is increased by an order of magnitude the power in the outflows is self-limiting, similar to the cross-polar potential. The peak power level is reached at an O^+ concentration of $\sim 25-50\%$ attaining a value of $\sim 1/3$ of the power in the Joule heating of the ionosphere. This result is significant in that we are able to account for a substantial fraction of the energy input into the ionosphere and that this energy input reappears as energy output in the form of enhanced ionospheric outflows. Of equal importance is the fact the energy has to be carried by heavy ionospheric ions and not light ions because of the restrictions on the speed of the outflows associated with feedback from the cross-polar cap potential.

7. Summary

[46] The 24–25 September 1998 magnetic cloud event is significant in that it was observed to produce a substantial increase in the ionospheric outflow rate that the mantle was dominated by plasma of ionospheric origin [*Moore et al.*, 1999]. The event was also sufficiently well observed that there are quantitative estimates for the cross-polar cap potential and auroral power input from AMIE and Polar UVI. This comprehensive data set has been used in this paper to quantify the global effects that the enhanced ionospheric outflows might have on the magnetosphere. A key factor in assessing the influence of ionospheric ions is the use of multifluid simulations that are able to separately tract the solar wind protons, light ionospheric ions (H^+) and heavy ionospheric ions (O^+). A fourth fluid that comprises the electrons irrespective of their origin provides quasineutrality.

[47] It is shown that if the ionospheric outflow of both H^+ and O^+ are substantially smaller than the statistical rates report by *Yau and André* [1997], then the model cross-polar cap potential tends to be substantially higher than the potential calculated by AMIE. However, as the outflow rates approach the statistical values for both the ionospheric H^+ and O^+ ions, the model potentials converge on the AMIE potential.

[48] The O^+ ions play a crucial role in the cross-polar cap potential because even though their number density may only be comparable to the H^+ density, they add substantial mass to the magnetosphere. Because there is only a limited amount of momentum flux transferred to the magnetosphere, this mass loading reduces the net convection speed within the magnetosphere and hence limits the value attained by the cross-polar cap potential. While ionospheric outflows have previously been suggested as being an important source of plasma to the magnetosphere, the results presented here are the first to demonstrate the vital consequences that these outflows might have in the overall convection patterns induced within the magnetosphere.

[49] There were several other independent checks made to verify whether the model outflow rates where consistent with other characteristics observed during the event. One was the position of the open/closed boundary relative the Polar UVI images. The model results indicate that the presence of strong heavy ionospheric outflows can shift the boundary by several degrees, and the best fit with the UVI data was attained when the outflow rates were comparable to the *Yau and André* [1997] fluxes.

[50] Similarly, we investigated the balance between the power input as determine by UVI and AMIE, relative to the power output derived from the model outflows. The calculations show that an ionospheric plasma with only H^+ present has a significant imbalance between the energy input and the power output. Ionospheric O^+ ions provide a crucial energy sink, and the power in the model outflows is comparable to the energy input determined by UVI and AMIE when the outflow rates are close to the *Yau and André* [1997] values.

[51] In summary, the presence of heavy ionospheric outflows has macroscopic effects on the global dynamics of the magnetosphere, including limiting the cross-polar cap potential, providing a substantial sink for the energy flowing into the auroral region, modifying the open/closed boundary and in determine the distribution of energetic particles in the magnetosphere. The ionospheric outflows lead to considerable structure in the magnetosphere. The modeling that has outflow rates comparable to the values of *Yau and André* [1997] show for this event an LLBL that is dominated by plasma of solar wind origin, and the tail in the midnight sector in the near-Earth region (i.e., the plasma sheet) by ionospheric ions, and in between a region where the density may be dominated by ions of solar wind origin, but the hot component is dominated by ionospheric ions and in some regions dominated by hot O^+ ions.

References

André, M., and A. Yau, Theories and observations of ion energization and outflow in the high latitude magnetosphere, *Space Sci. Rev.*, *80*, 27, 1997.

Borovsky, J. E., M. F. Thomsen, and D. J. McComas, The superdense plasma sheet: Plasmaspheric origin, solar wind origin, or ionospheric origin?, *J. Geophys. Res.*, *102*, 22,089, 1997.

Chappell, C. R., T. E. Moore, and J. H. Waite Jr., The ionosphere as a fully adequate source of the Earth's magnetosphere, *J. Geophys. Res.*, *92*, 5896, 1987.

Chappell, C. R., B. L. Giles, T. E. Moore, D. E. Delcourt, P. D. Craven, and M. O. Chandler, The adequate of the ionospheric sources in supplying magnetospheric plasma, *J. Atmos. Sol. Terr. Phys.*, *62*, 421, 2000.

Cladis, J. B., Parallel acceleration and transport of ions from polar ionosphere to plasma sheet, *Geophys. Res. Lett.*, *13*, 893, 1986.

Delcourt, D. C., C. R. Chappell, T. E. Moore, and J. H. Waite Jr., A three-dimensional numerical model of ionospheric plasma in the magnetosphere, *J. Geophys. Res.*, *94*, 11,893, 1989.

Delcourt, D. C., J. A. Sauvaud, and T. E. Moore, Polar wind ion dynamics in the magnetotail, *J. Geophys. Res.*, *98*, 9155, 1993.

Fedder, J. A., S. P. Linker, and J. G. Lyon, A comparison of global numerical simulation results to data for the January 27–28, 1992, geospace environment challenge event, *J. Geophys. Res.*, *103*, 14,799, 1998.

Hamilton, D. C., G. Gloeckler, F. M. Ipovitch, W. Studenmann, B. Wilken, and G. Kremser, Ring current development during the great geomagnetic storm of February, 1986, *J. Geophys. Res.*, *93*, 14,343, 1988.

Hirahara, M., T. Mukai, T. Terasawa, S. Machida, Y. Saito, T. Yamamoto, and S. Kokubun, Cold dense ion flows with multiple components observed in the distant tail lobe by Geotail, *J. Geophys. Res.*, *101*, 7769, 1996.

Horwitz, J. L., Core plasma in the magnetosphere, *Rev. Geophys.*, *25*, 579, 1987.

Johnson, R. G., Energetic ion composition in the Earth's magnetosphere, *Rev. Geophys.*, *17*, 696, 1979.

Krimigis, S. M., G. Gloeckler, R. W. McEntire, T. A. Potemra, F. L. Scarf, and E. G. Shelley, Magnetic storm of September 4, 1984: A synthesis of ring current spectra and energy densities measured with AMPTE/CCE, *Geophys. Res. Lett.*, *12*, 329, 1985.

Lennartsson, W., Plasma sheet ion composition at various levels of geomagnetic and solar activity, *Phys. Scr.*, *36*, 367, 1987.

Lennartsson, W., A scenario for solar wind penetration of Earth's magnetic tail based on ion composition data from the ISEE 1 spacecraft, *J. Geophys. Res.*, *97*, 19,221, 1992.

Lu, G., et al., High-latitude ionospheric electrodynamics as determined by the assimilative mapping of ionospheric electrodynamics procedure for the conjunctive SUNDIAL/ATLAS 1/GEM period of March 28–29, 1992, *J. Geophys. Res*, *101*, 26,697, 1996.

Moore, T. E., Origins of magnetospheric plasma, *Rev. Geophys.*, *29*, 1039, 1991.

Moore, T. E., and D. C. Delcourt, The geopause, *Rev. Geophys.*, *33*, 175, 1995.

Moore, T. E., W. K. Peterson, C. T. Russell, M. O. Chandler, M. R. Collier, H. L. Collin, P. D. Craven, R. Fitzenreiter, B. L. Giles, and C. J. Pollock, Ionospheric mass ejection in response to a CME, *Geophys. Res. Lett.*, *26*, 2339, 1999.

Mukai, T., M. Hirahara, S. Machida, Y. Saito, T. Terasawa, and A. Nishida, Geotail observation of cold ion streams in the medium distance magnetotail lobe in the course of a substorm, *Geophys. Res. Lett.*, *21*, 1023, 1994.

Raeder, J., J. Berchem, and M. Ashour-Abdalla, The Geospace Environment Modeling grand challenge: Results from a global geospace circulation model, *J. Geophys. Res.*, *103*, 14,787, 1998.

Roeder, J. L., J. F. Fennell, M. W. Chen, M. Schulz, M. Grande, and S. Livi, CRRES observations of the composition of the ring-current ion populations, *Adv. Space Res.*, *17*, 17, 1996.

Seki, K., M. Hirahara, T. Terasawa, I. Shinohara, T. Mukai, Y. Saito, S. Machida, T. Yamamoto, and S. Kokubun, Coexistence of Earth-origin O^+ and solar wind-origin H^+/He^{++} in the distant magnetotail, *Geophys. Res. Lett.*, *23*, 985, 1996.

Seki, K., M. Hirahara, T. Terasawa, T. Mukai, Y. Saito, S. Machida, T. Yamamoto, and S. Kokubun, Statistical properties and possible supply mechanisms of tailward cold O^+ beams in the lobe/mantle regions, *J. Geophys. Res.*, *103*, 4477, 1998.

Terasawa, T., et al., Solar wind control of density and temperature in the near-Earth plasma sheet: WIND/GEOTAIL collaboration, *Geophys. Res. Lett.*, *24*, 935, 1997.

Yau, A. W., and M. André, Source of ion outflow in the high latitude ionosphere, *Space Sci. Rev.*, *80*, 1, 1997.

Winglee, R. M., Multi-fluid simulations of the magnetosphere: The identification of the geopause and its variation with IMF, *Geophys. Res. Lett.*, *25*, 4441, 1998a.

Winglee, R. M., Imaging the ionospheric and solar wind sources in the magnetosphere through multi-fluid global simulations, *Phys. Space Plasmas*, *15*, 345,1998b.

Winglee, R. M., Mapping of ionospheric outflows into the magnetosphere for varying IMF conditions, *J. Atmos., Sol. Terr. Phys.*, *62*, 527, 2000.

Winglee, R. M., V. O. Papitashvili, and D. R. Weimer, Comparison of the high-latitude ionospheric electrodynamics inferred from global simulations and semiempirical models for the January 1992 GEM Campaign, *J. Geophys. Res.*, *102*, 26,961, 1997.

———————————

M. Brittnacher, D. Chua, G. K. Parks, and R. M. Winglee, Geophysics Program, Box 35160, University of Washington, Seattle WA 98195-1650, USA. (winglee@geophys.washington.edu)

G. Lu, National Center for Atmospheric Research, Boulder, CO 80307, USA.